Results in Engineering 15 (2022) 100593

Contents lists available at ScienceDirect

Results in Engineering

journal homepage: www.sciencedirect.com/journal/results-in-engineering

Improving extreme response prediction of a subsea shuttle tanker hovering in ocean current using an alternative highly correlated response signal

Oleg Gaidai [a], Yihan Xing [b,*], Rajiv Balakrishna [b]

[a] Shanghai Engineering Research Centre of Marine Renewable Energy, College of Engineering Science and Technology, Shanghai Ocean University, Shanghai, China
[b] Department of Mechanical and Structural Engineering and Materials Science, University of Stavanger, Norway

ARTICLE INFO

Keywords:
Subsea technology
Submarine
LQR
Bivariate correction method
Extreme responses
Bivariate probability distribution

ABSTRACT

A subsea shuttle tanker (SST) is a pioneering underwater submarine specifically designed to economically transport CO2 to smaller hydrocarbon fields. During loading and unloading of the CO2, the SST hovers over the well and experiences extreme heave motions resulting in extreme hydrostatic loading. Sustaining the hydrostatic loading is indispensable as it forms the dominating load and is a driving factor determining the SST hull's collapse design. Furthermore, the SST's extreme surge motion regulates the length of the flowline to evade snap loads. This paper focuses on the problem of determining these extreme positional responses at one location when the aft thruster fails during offloading using data with a shorter time record from another location at the SST. This scenario could be of practical engineering importance when either one of the sensors is malfunctioning or another similar vessel is being designed for the same environmental condition. A 2D planar Simulink model is used to generate the empirical data required for the study.

1. Introduction

The subsea shuttle tanker (SST), as presented in Ref. [1], is an innovative and novel autonomous submarine proposed by Equinor in two of their research disclosures in Equinor [2] and Ellingsen et al. [3]. The baseline SST targets ongoing carbon capture and storage (CCS) projects in Norway. Such projects are enacted in Sleipner, Utgard, and Snøhvit [4]. The CO_2 is transferred from an onshore site and stored in the SST before being hauled away autonomously to a subsea well for direct injection. The SST, which cruises at a depth of 70 m, can function in any weather condition since it moves in depths unaffected by winds or wave loads. The primary function of the SST is to provide CO_2 transportation to the marginal fields since it is more economically viable than using offshore pipelines or ship tankers. Recent feasibility studies by Xing et al. [5]; considering SSTs designed using DNVGL-RU-NAVAL-Pt4Ch1 [6]; have shown that the SST is economically more attractive in smaller CO_2 fields. Primary design parameters for the baseline SST [1] are given in Table 1.

After navigating through the waters and reaching its destination, the SST will hover steadily and commence its operation with the help of a flexible flowline established by a remotely operated vehicle (ROV). The methodology of the offloading process is presented in Fig. 1. Throughout this procedure, the position of the SST will be maintained dynamically by its propeller and thrusters coordinating with a Linear Quadratic Regulator (LQR) control system to mitigate any positional disturbances [8] due to the environmental loads from ocean currents (presented in Fig. 2).

The extreme hydrostatic loads experienced by the SST during its operation are determined by the extreme heave and pitch values and are the driving force that leads to the collapse of the SST pressure hull. Ensuring these values' reliability is even more critical in case of thruster failure and is exemplified in this paper by considering the aft thruster failure scenario. In such a failure scenario, the SST will lose its manoeuvrability, resulting in more significant responses. Moreover, only the fore thruster provides the power, resulting in an unbalance with the global resulting thruster forces, substantial pitch responses and aft heave motions. This failure demonstrates the importance of ensuring that these values are accurately calculated. In this paper, extreme responses of the SST during unloading during the failure of the aft thruster are examined at locations 2 and 3 (see Fig. 1). Two different current velocities of 0.5 and 1.0 m/s are used with the bivariate Gumbel copula and bivariate correction method. The bivariate correction method has been widely used in many applications, for example, to obtain maximum structural responses [9–15] and extreme wind and wave profiles

* Corresponding author.
E-mail address: yihan.xing@uis.no (Y. Xing).

https://doi.org/10.1016/j.rineng.2022.100593
Received 7 July 2022; Received in revised form 12 August 2022; Accepted 13 August 2022
Available online 24 August 2022

Table 1
Main design parameters of the baseline SST.

Parameter	Value	Unit
Length	164	m
Beam	17	m
Weight	3.36×10^7	kg
Center of buoyancy (CoB) $[x_b, y_b, z_b]$	[0, 0, −0.41]	m
Skeg position x_s	67	m
Skeg area A_S	40	m^2
Forward tunnel thruster position x_{tf}	60	m
Aft tunnel thruster position x_{ta}	−60	m
CO_2 cargo capacity	1.7×10^6	kg
Operating depth	70	m

[16–18], extreme wave heights [19], and extreme current profiles [20]. At the same time, the bivariate correction method uses the inherent model of non-linearities without any simplifications. This method is from the Monte Carlo method and makes it highly relevant when used to solve the highly non-linear SST motion calculation in this paper. This paper generates the empirical data with time-domain simulations from a 2D planar Simulink model (Section 2). For more details on extreme response prediction improvement using alternative highly correlated response signals, see Wang [21]; Gaidai et al. [16,17] and Xu et al. [15].

2. Simulink model implementation

The Simulink model used in this paper was developed by Ma et al. [8, 22] and is presented in Fig. 3 and Fig. 4. Further, short descriptions of the Simulink model are presented in the following sub-section below.

The Simulink model is build-up using the below-mentioned blocks:

- Plant model: The plant model is a replica of the SST enacting the equation of motions, including a variety of forces such as drag and lift forces, and hydrostatics and hydrodynamic derivatives

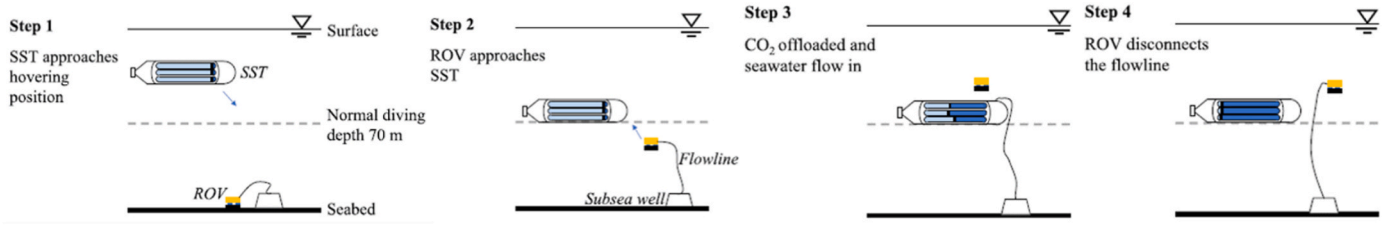

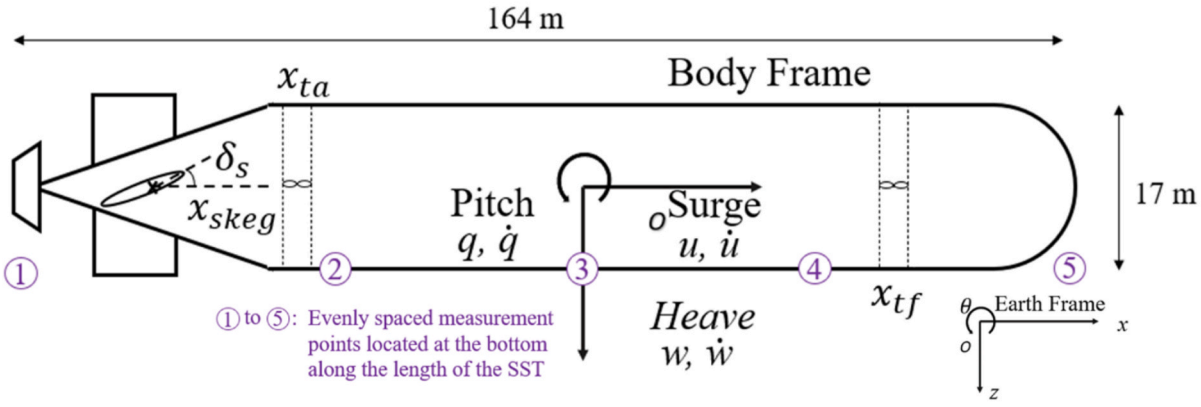

Fig. 1. SST offloading sequence [1,7].

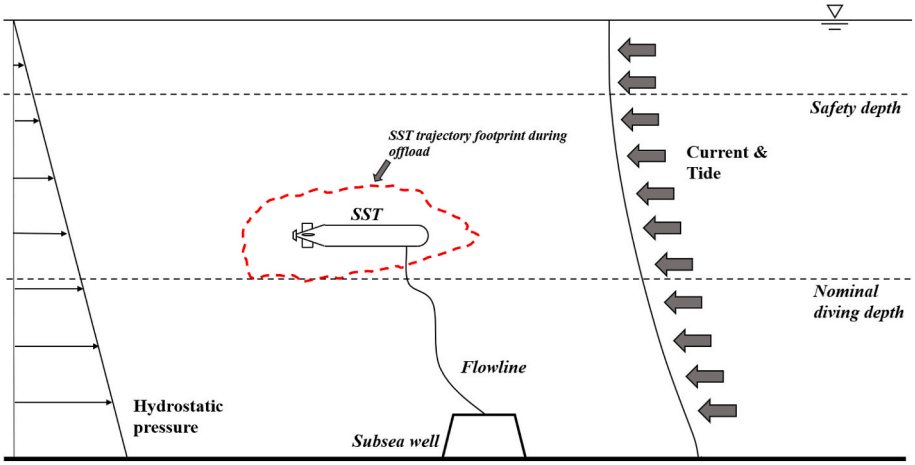

Fig. 2. SST subjected to environmental loads during offloading [7].

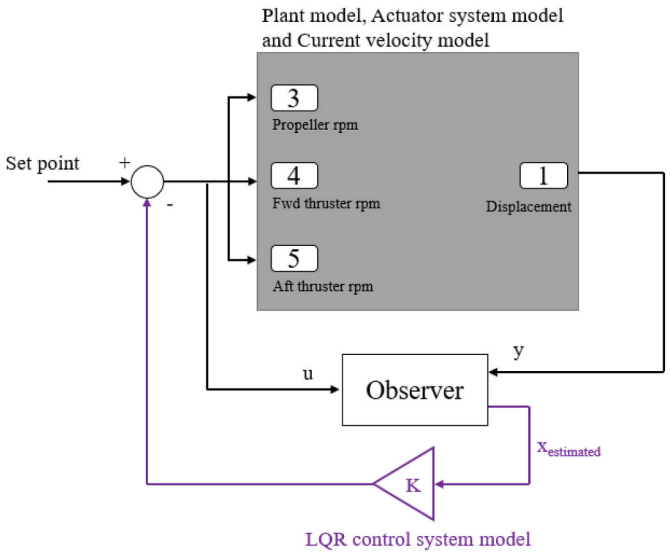

Fig. 3. Simulink model implementation – Control system model feedback loop [7].

- Actuator system model: The actuator system model enacts the ballast tanks', the propeller's, and thrusters' forces and moments.
- LQR control system model: A LQR control system is replicated through this model
- Observer: An Luenberger [23] Observer is replicated through this block.
- Current velocity model: The ocean current velocities are replicated in this model.

The Simulink model, with its respective blocks acting as the control system and feedback loops model, enables the evaluation of the response loads, which is then used for the bivariate analysis in this paper.

3. Mathematical bivariate model

In this section original mathematical bivariate model as in Gaidai et al. (2018, [13,16,17,19,24–26]; Sun et al. [27]; Xing et al. [28], Xu et al. [29] is briefly introduced. The key advantage of this model is its ability to identify the effect of dependency between the time series data on the extreme value distribution. Also, the whole time series can be used as input data without de-cluttering (i.e., no requirement to use independent data). However, the most prominent feature of the model is its ability to provide a non-parametric depiction of the extreme value distribution inherent in the data. Therefore, this paper looks at the long-term global response process X(t) of the submarine hull, calculated through a time interval between $(0, T)$. The eventual bivariant values have been calculated in this paper as described in Refs. [16–18].

As already mentioned, the method proposed in this paper will be based on the bivariate correction methodology. This involves both the univariate and bivariate ACER functions.

For a stationary stochastic process $X(t)$, that has been measured over a specific time interval $(0,T)$, there are discrete process values $X_1, \ldots, X_N$ That have been measured/simulated at equidistant time moments $t_1, \ldots, t_N$ in $(0, T)$. The latter discrete process values could be precisely observed values of $X(t)$ at each t_j, $j = 1, \ldots, N$, or it could be maxima values over time intervals centred at the t_j's. The target is to accurately estimate the cumulative distribution function (CDF) of the extreme value $M_N = \max\ \{X_j ; j = 1, \ldots, N\}$. Equivalently, we want to estimate $CDF(\eta) = \text{Prob}(M_N \le \eta)$ for large values of η. According to the definition of CDF (η)

$$\text{CDF}(\eta) = \text{Prob}(M_N \le \eta) = \text{Prob}\{X_N \le \eta, \ldots, X_1 \le \eta\}$$

$$= \text{Prob}\{X_N \le \eta | X_{N-1} \le \eta, \ldots, X_1 \le \eta\} \cdot \text{Prob}\{X_{N-1} \le \eta, \ldots, X_1 \le \eta\}$$

$$= \prod_{j=2}^{N} \text{Prob}\{X_j \le \eta | X_{j-1} \le \eta, \ldots, X_1 \le \eta\} \cdot \text{Prob}(X_1 \le \eta) \quad (1)$$

If all the X_j can be regarded as statistically independent, then

$$\text{CDF}(\eta) \approx \prod_{j=1}^{N} \text{Prob}(X_j \le \eta) \quad (2)$$

In most cases, the dependence between the X_j's exists and is not negligible; therefore, the following one-step memory approximation is introduced

$$\text{Prob}\{X_j \le \eta | X_{j-1} \le \eta, \ldots, X_1 \le \eta\} \approx \text{Prob}\{X_j \le \eta | X_{j-1} \le \eta\} \quad (3)$$

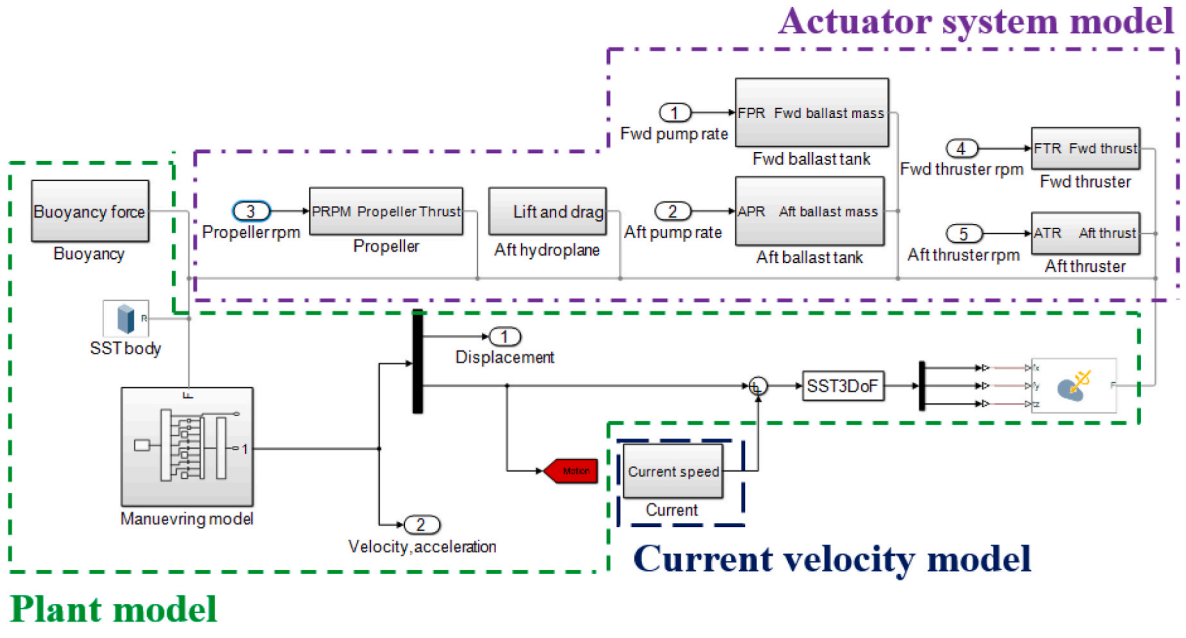

Fig. 4. Simulink model implementation – Plant model, Actuator system model and Current velocity model [7].

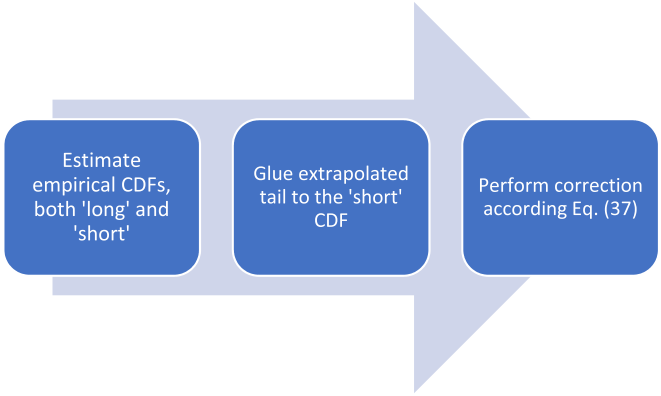

Fig. 5. Correction scheme.

for $2 \le j \le N$. The next approximation can be expressed as

$$\text{Prob}\{X_j \le \eta | X_{j-1} \le \eta, \ldots, X_1 \le \eta\} \approx \text{Prob}\{X_j \le \eta | X_{j-1} \le \eta, X_{j-2} \le \eta\} \tag{4}$$

where $3 \le j \le N$, and so on. Eqs. (2) and (3) represent refinements of the independence assumption. Such approximations are able to capture the effect of statistical dependence between neighbouring data points in the time series with increasing accuracy. Combining Eq. (1) with Eq. (2), the following approximation is introduced

$$\text{CDF}(\eta) \approx \frac{\prod_{j=2}^{N} p_{2j}(\eta)}{\prod_{j=2}^{N-1} p_{1j}(\eta)} \tag{5}$$

with the following notation $p_{kj}(\eta) = \text{Prob}\{X_j \le \eta, \ldots, X_{j-k+1} \le \eta\}$ for $j \ge k$.

It is of interest to study closer the values for CDF (η)

$$\text{CDF}(\eta) \approx \prod_{j=1}^{N} (1 - \alpha_{1j}(\eta)), \tag{6}$$

where

$$\alpha_{1j}(\eta) = \text{Prob}\{X_j > \eta\} = 1 - p_{1j}(\eta). \tag{7}$$

Thus

$$\text{CDF}(\eta) \approx \text{CDF}_1(\eta) = \exp\left(-\sum_{j=1}^{N} \alpha_{1j}(\eta)\right), \tag{8}$$

Alternatively, Eq. (6) gives

$$\text{CDF}(\eta) \approx \prod_{j=2}^{N} (1 - \alpha_{2j}(\eta))\, p_{11}(\eta), \tag{9}$$

where $\alpha_{kj}(\eta) = 1 - p_{kj}(\eta)/p_{k-1\,j-1}(\eta)$, for $j \ge k \ge 2$. That is

$$\alpha_{kj}(\eta) = \text{Prob}\{X_j > \eta \mid X_{j-1} \le \eta, \ldots, X_{j-k+1} \le \eta\} \tag{10}$$

denotes the exceedance probability, being conditional on $k-1$ previous non-exceedances. From Eq. (8) it is obtained that

$$\text{CDF}(\eta) \approx \text{CDF}_2(\eta) = \exp\left(-\sum_{j=2}^{N} \alpha_{2j}(\eta) - \alpha_{11}(\eta)\right), \tag{11}$$

since $p_{11}(\eta) \approx \exp(-\alpha_{11}(\eta))$. Conditioning on the two previous observations X_{j-2}, X_{j-1} preceding X_j gives

$$\text{CDF}(\eta) \approx \text{CDF}_3(\eta) = \exp\left(-\sum_{j=3}^{N} \alpha_{3j}(\eta) - \alpha_{22}(\eta) - \alpha_{11}(\eta)\right), \tag{12}$$

and so on. Thus, extreme value prediction by the conditioning approach introduced above reduces to the estimation of the $\alpha_{kj}(\eta)$ functions. For most applications $N \gg k$, so that $\sum_{j=1}^{k-1} \alpha_{jj}(\eta)$ is, in fact, negligible compared to $\sum_{j=k}^{N} \alpha_{kj}(\eta)$. Thus, for most cases, the following approximation is valid

$$\text{CDF}_k(\eta) \approx \exp\left(-\sum_{j=k}^{N} \alpha_{kj}(\eta)\right), k \ge 1\,. \tag{13}$$

Next, the concept of average conditional exceedance rate (ACER) of order k can be introduced

$$\varepsilon_k(\eta) = \frac{1}{N-k+1} \sum_{j=k}^{N} \alpha_{kj}(\eta)\,, k = 1, 2, \ldots \tag{14}$$

Finally, the following random functions can be introduced

$$A_{kj}(\eta) = 1\{X_j > \eta, X_{j-1} \le \eta, \ldots, X_{j-k+1} \le \eta\}\,, j = k, \ldots, N, k = 2,\ 3, \ldots \tag{15}$$

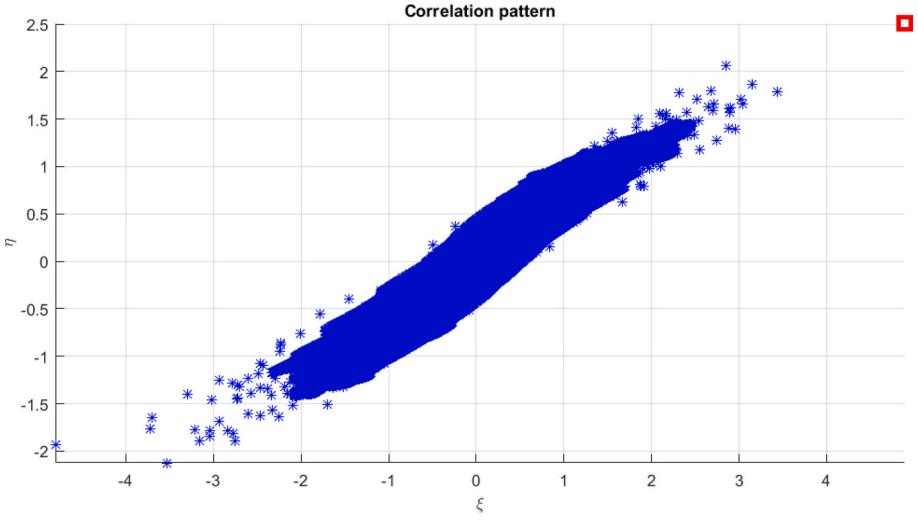

Fig. 6. Phase space between simulated R_2 and R_3 SST vessel responses. The red square indicates the predicted extreme value. (For interpretation of the references to colour in this figure legend, the reader is referred to the Web version of this article.)

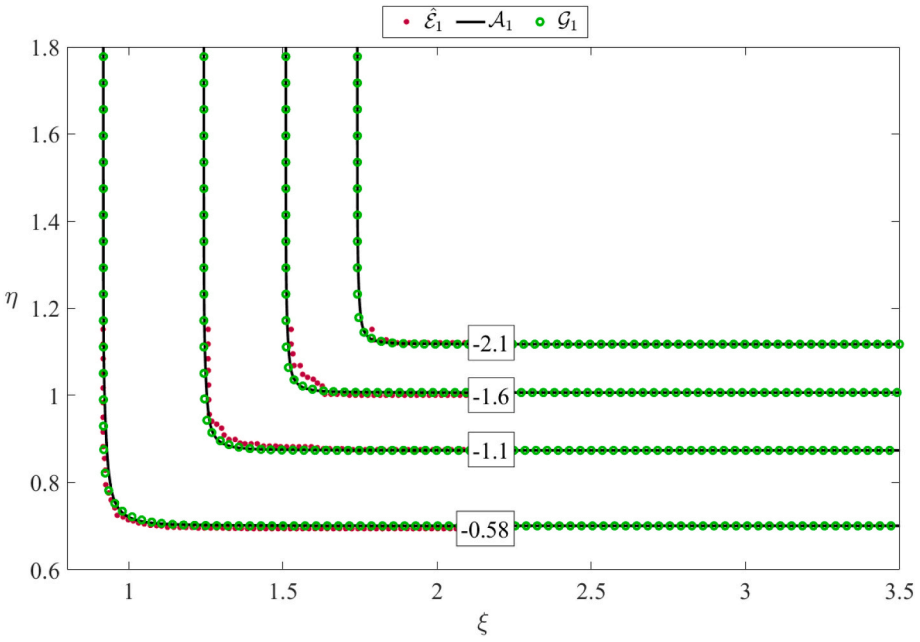

Fig. 7. A Gumbel copula fit versus the empirical bivariate ACER function for the lighthouse data. Red dots indicate the empirical ACER function, green circles the Gumbel logistic model, and the solid line indicates the Asymmetric Gumbel logistic model. Negative numbers indicate probability levels on the decimal logarithmic scale. (For interpretation of the references to colour in this figure legend, the reader is referred to the Web version of this article.)

and

$$B_{kj}(\eta) = 1\{X_{j-1} \le \eta, \ldots, X_{j-k+1} \le \eta\}\ , j = k, \ldots, N, k = 2,\ 3, \ldots\ , \tag{16}$$

where $1\{\mathscr{A}\} = 1$ if $\mathscr{A}$ is true, while it is zero if not. Then

$$\alpha_{kj}(\eta) = \frac{\mathbb{E}[A_{kj}(\eta)]}{\mathbb{E}[B_{kj}(\eta)]}\ , j = k, \ldots, N, k = 2, \ldots\ , \tag{17}$$

where $\mathbb{E}[\cdot]$ denotes the expectation operator. Obviously, $\lim_{\eta\to\infty}\mathbb{E}[B_{kj}(\eta)] = 1$. Thus, $\lim_{\eta\to\infty}\widetilde{\varepsilon}_k(\eta)/\varepsilon_k(\eta) = 1$, where

$$\widetilde{\varepsilon}_k(\eta) = \frac{\sum_{j=k}^{N}\mathbb{E}[A_{kj}(\eta)]}{N-k+1}\ . \tag{18}$$

To prove why previous equations may be applicable for non-stationary time series, it is seen that

$$\mathrm{CDF}_k(\eta) \approx \exp\left(-\sum_{j=k}^{N}\alpha_{kj}(\eta)\right) = \exp\left(-\sum_{j=k}^{N}\frac{\mathbb{E}[A_{kj}(\eta)]}{\mathbb{E}[B_{kj}(\eta)]}\right)$$

$$\approx \exp\left(-\sum_{j=k}^{N}\mathbb{E}[A_{kj}(\eta)]\right), \eta\to\infty\ . \tag{19}$$

If the time series can be split into K blocks such that $\mathbb{E}[A_{kj}(\eta)]$ remains approximately constant within each span block and such that $\sum_{j\in C_i}\mathbb{E}[A_{kj}(\eta)] \approx \sum_{j\in C_i}a_{kj}(\eta)$ for a sufficient range of η-values, where C_i denotes the set of indices for block no. i, $i = 1, \ldots, K$, and where $a_{kj}(\eta)$ are the realized values of $A_{kj}(\eta)$ for the observed time series, then $\sum_{j=k}^{N}\mathbb{E}[A_{kj}(\eta)] \approx \sum_{j=k}^{N}a_{kj}(\eta)$. Therefore, for a recorded time series of a non-stationary process that complies with the stated conditions, it follows that

$$\mathrm{CDF}_k(\eta) \approx \exp\ \left(-(N-k+1)\widehat{\varepsilon}_k(\eta)\right)\ , \tag{20}$$

where

$$\widehat{\varepsilon}_k(\eta) = \frac{1}{N-k+1}\sum_{j=k}^{N}a_{kj}(\eta) \tag{21}$$

Now let one consider the scatter diagram of $m = 1, \ldots, M$ sea states, each sea state having a probability p_m, such that $\sum_{m=1}^{M}p_m = 1$. Next, introduce the long-term ACER function of order k, defined as,

$$\mathrm{ACER}_k(\eta) \equiv \sum_{m=1}^{M}\widehat{\varepsilon}_k(\eta, m)p_m \tag{22}$$

with $\widehat{\varepsilon}_k(\eta, m)$ is the same function as in Eq. (21), but corresponds to a specific sea state number m. The long-term extreme value distribution of $M(T)$, based on the ACER function of order k, can be expressed as follows

$$\mathrm{Prob}(M(T) \le \eta) \approx \exp(-N \cdot \mathrm{ACER}_k(\eta)) \tag{23}$$

where $\widehat{\varepsilon}_k(\eta)$ is the empirical ACER function of order k, with $k \ll N$; N is a total number of data in the analyzed time series.

Now, consider a bivariate stochastic process $Z(t) = (X(t), Y(t))$ with dependent component processes, which has been observed over a time interval, $(0, T)$ say. Assume that the sampled values $(X_1, Y_1), \ldots, (X_N, Y_N)$ are allocated to the (usually equidistant) discrete times $t_1, \ldots, t_N$ in $(0, T)$. Our goal in this paper is to accurately determine the joint distribution function of the extreme value vector $(\widehat{X}_N, \widehat{Y}_N)$, where $\widehat{X}_N = \max\{X_j; j = 1, \ldots, N\}$, and with a similar definition of $\widehat{Y}_N$. Specifically, we want to estimate $P(\xi, \eta) = Prob(\widehat{X}_N \le \xi, \widehat{Y}_N \le \eta)$ accurately for large values of ξ and η.

For notational convenience, it is expedient to introduce the non-exceedance event $\mathscr{C}_{kj}(\xi, \eta) = \{X_{j-1} \le \xi, Y_{j-1} \le \eta, \ldots, X_{j-k+1} \le \xi, Y_{j-k+1} \le \eta\}$ for $1 \le k \le j \le N+1$. Then, from the definition of $P(\xi, \eta)$ it

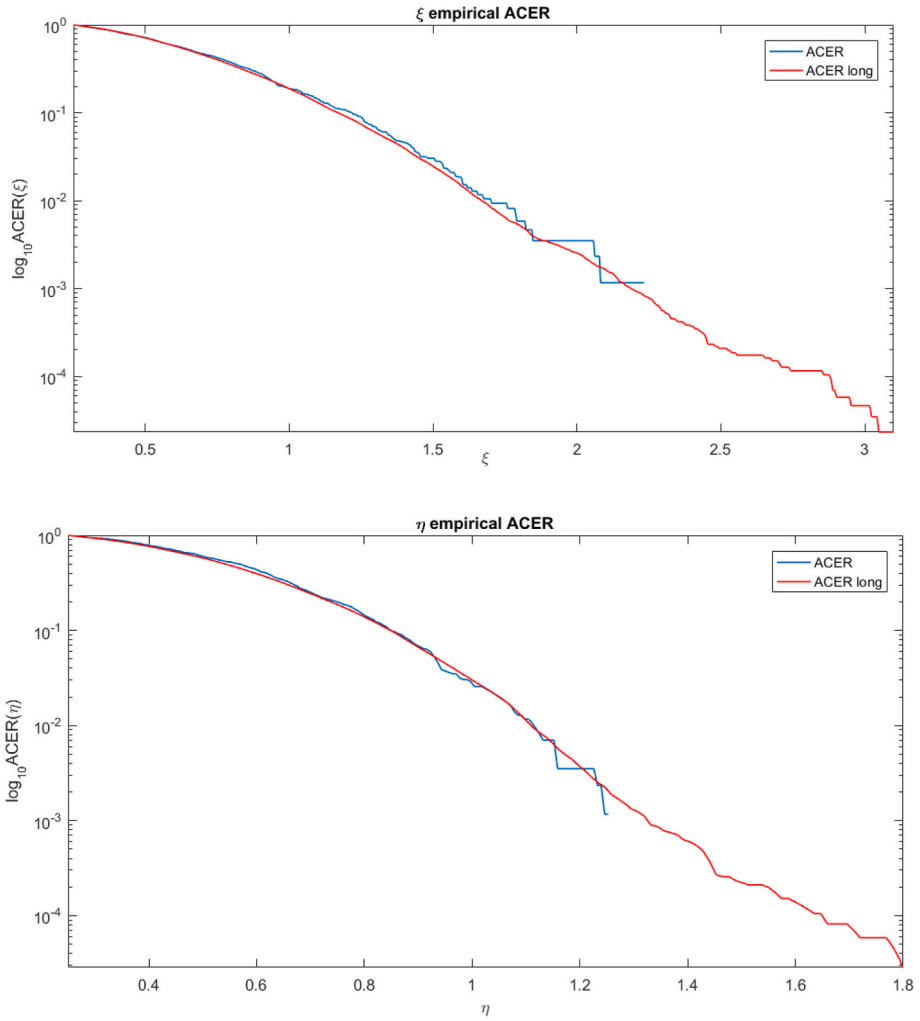

Fig. 8. ACER functions for shorter and longer SST response records: R_2 and R_3 vessel responses, upper and lower figures, respectively. The ACER function decimal logarithm values are on the vertical axes.

Table 2
Correction results for measured SST vessel response: 80 h (long) and 0.8 h (short). 40 days return period prediction.

	Current = 0.5 m/s	Current = 1 m/s
$R_{3\text{short}}/\ R_{3\text{long}}$	1.17	1.20
$R_{3\text{corrected}}/\ R_{3\text{long}}$	1.02	1.03

follows that

$$P(\xi,\eta) = Prob\left(\mathscr{C}_{N+1,N+1}(\xi,\eta)\right)$$
$$= Prob(X_N \le \xi, Y_N \le \eta |\ \mathscr{C}_{NN}(\xi,\eta)) \cdot Prob(\mathscr{C}_{NN}(\xi,\eta)) = \prod_{j=2}^{N} \text{Unsupported} \quad Prob\left(X_j \le \xi, Y_j \le \eta \middle|\ \mathscr{C}_{jj}\left(\xi,\eta\right) \cdot Prob\left(\mathscr{C}_{22}\left(\xi,\eta\right)\right)\right) \tag{24}$$

Based on Eq. (24) and the properties of conditional probability, a sequence of approximations may be introduced which converges to the target distribution $P(\xi,\eta)$. In practice, it is therefore assumed that the following representation applies to a suitably chosen k:

$$P(\xi,\eta) \approx \exp\left\{-\sum_{j=k}^{N}\left(\alpha_{kj}(\xi;\eta) + \beta_{kj}(\eta;\xi) - \gamma_{kj}(\xi,\eta)\right)\right\}; \quad \xi,\eta \to \infty, \tag{25}$$

where we have used the notation $\alpha_{kj}(\xi;\eta) = Prob(X_j > \xi |\ \mathscr{C}_{kj}(\xi,\ \eta))$, $\beta_{kj}(\eta;\xi) = Prob(Y_j > \eta |\ \mathscr{C}_{kj}(\xi,\eta))$ and $\gamma_{kj}(\xi,\eta) = Prob(X_j > \xi, Y_j > \eta |\ \mathscr{C}_{kj}(\xi,\eta))$. Note that Eq. (2) applies equally well to stationary and non-stationary time series. This is due to the fact that the possible time dependence of the conditional exceedance probabilities $\alpha_{kj}(\xi;\eta)$, $\beta_{kj}(\eta;\xi)$ and $\gamma_{kj}(\xi,\eta)$ has been retained, which is reflected in the presence of the time parameter j.

From Eq. (25) it emerges that for the estimation of the bivariate extreme value distribution, it is necessary and sufficient to estimate the sequence of functions $\{\alpha_{kj}(\xi;\eta) + \beta_{kj}(\eta;\xi) - \gamma_{kj}(\xi,\eta)\}_{j=k}^{N}$. To get a more compact representation, it is expedient to introduce the concept of k'th

order bivariate average conditional exceedance rate (ACER) function as follows,

$$\mathscr{E}_k(\xi,\eta)=\frac{1}{N-k+1}\sum_{j=k}^{N}\left(\alpha_{kj}(\xi;\eta)+\beta_{kj}(\eta;\xi)-\gamma_{kj}(\xi,\eta)\right);\quad k=1,2,\ldots \tag{26}$$

The unique feature of the ACER functions is that they provide the possibility to portray the exact extreme value distribution inherent in the data time series, both the univariate and the bivariate [9,10,13,14]. Hence, the bivariate correction method is fundamentally different from the traditional approach relying on the fitting of hardly asymptotic data to asymptotic extreme value distributions, which, in fact, are based on the assumption of stationary time series as opposed to the bivariate correction method. The empirical ACER functions are represented in the form of non-parametric numerical functions with uncertainty bounds. The accuracy obtained depends, of course, on the amount of data available to estimate these functions. It is also an essential feature of the bivariate correction method that it is not limited to stationary time series. It is entirely valid for non-stationary time series as long as the measured data reflects this non-stationarity.

This section presents a statistical bivariate integral correction that is based on the bivariate correction method coupled with the Gumbel logistic model [9,10,13–17,21]. Note that this correction is not limited to only extreme value estimates, but it can be applied with appropriate bivariate models for any statistical values of interest to improve their accuracy based on synchronously measured longer, highly correlated data records.

Let $X=\max\{R_2(t);t\in[0,T_{\text{return}}]\}$, $Y=\max\{R_3(t);t\in[0,\ T]\}$, where R_2, R_3 are responses measured at channels number 2 and 3 correspondingly, see Fig. 1, with T being the return period of interest, and let $F_{XY}(\xi,\eta)=Prob(X\le\xi,Y\le\eta)$ be the joint bivariate cumulative distribution function (CDF) of (X,Y).

Raw response time series with $dt=0.0246$ sec were blocked into $k=50$ consecutive discrete time points maxima to reduce the neighbouring data points' correlation effect. The conditioning level k was selected according to the response power spectral density because this level in the distribution tail resulted in a good convergence of the ACER functions (Section 3).

$F_X(\xi)$ and $F_Y(\eta)$ denote the corresponding univariate marginal CDFs for X and Y, respectively. In this paper, it is assumed that the bivariate couple $(R_2(t),\ R_3(t))$ has been observed over a period of time $t\in[0,\widetilde{T}]$, where the observation duration $\widetilde{T}$ is not long enough for accurately predicting the univariate extreme response levels with a target low probability of interest. Now, consider the case when a 'long' record of $R_2(t)$ is available over a time $t\in[0,T]$, with $T\gg\widetilde{T}$, with a corresponding estimated CDF $F_X^{long}(\xi)$ of the CDF $F_X(\xi)$, which has a probability density function (PDF) $p_X=F_X^{'}$. In this paper $T_{\text{return}}\approx 40$ days is the return period that corresponds to the extreme probability p of interest, $p=10^{-6}$, $T=80$ h, $\widetilde{T}=T/100$ see Section 4. Then for any Y- response level of interest η_*, *with* $\Delta\to 0$,

$$F_Y(\eta_*)=F_{XY}(\infty,\eta)=\int_0^{+\infty}Prob(Y\le\eta_*|X=\xi)p_X(\xi)d\xi=\int_0^{+\infty}\frac{Prob(Y\le\eta_*,X\in[\xi,\ \xi+\Delta])}{Prob(X\in[\xi,\ \xi+\Delta])}p_X(\xi)d\xi=\int_0^{+\infty}F_{XY,X}^{'}(\xi,\eta_*)d\xi \tag{27}$$

with $F_{XY,X}^{'}(\xi,\eta)=\frac{\partial}{\partial\xi}F_{X,Y}(\xi,\eta)$. For the details related to these equations, see Wang [21]; Gaidai et al. [16,17] and Xu et al. [15]. The following copula model for the bivariate extreme value distribution is referred to as the Gumbel logistic model [9,10,13,14].

$$F_{XY}(\xi,\eta)=exp\left\{-\left[(-lnF_X(\xi))^m+(-lnF_Y(\eta))^m\right]^{1/m}\right\} \tag{28}$$

In this model, it is seen that $m=1$ corresponds to the case when X and Y are independent. When $0<m<1$, X and Y become dependent [9,10,13,14]. However, this dependence structure is of a special kind since it only involves the marginal distributions. Still, it appears to be useful in some practical cases. Another popular extreme value copula is the Asymmetric Gumbel logistic model, see Naess et al. [9,10]; Gaidai et al. [13] and Gao et al. [14]. This bivariate extreme value model will not be discussed further in this paper since it gives identical results to the Gumbel logistic model. The Gumbel logistic model has been verified to be a useful model for various offshore engineering practical applications, provided the marginal extreme value distributions are estimated using the univariate bivariate correction method instead of standard asymptotic extreme value distributions [9,10,13,14]. This is because the asymptotic distributions typically used are often not accurate enough in the tails, resulting in fitting real, sub-asymptotic data to asymptotic distributions. If Eq. (27) is differentiated with respect to ξ, it is obtained that

$$F_{XY,X}^{'}(\xi,\eta_*)=F_{XY}(\xi,\eta_*)[1+(ln\ F_Y(\eta_*)/ln\ F_X(\xi))^m]^{\frac{1}{m}-1}\frac{d}{d\xi}\ln F_X(\xi) \tag{29}$$

The numerical estimates $\widehat{F}_Y(\eta_*)$ and $\widehat{F}_{XY}(\xi,\eta_*)$ of $F_Y(\eta_*)$ and $F_{XY}(\xi,\eta_*)$, respectively, based on the available time series of recorded data, are now used in the following expression to obtain the corrected estimate $F_Y^{corr}(\eta_*)$

$$F_Y^{corr}(\eta_*)=\int_0^{+\infty}\widehat{F}_{XY}(\xi,\eta_*)\left[1+\left(ln\ \widehat{F}_Y\ (\eta_*)/ln\ \widehat{F}_X^{long}(\xi)\right)^m\right]^{\frac{1}{m}-1}\frac{d}{d\xi}\ln\widehat{F}_X^{long}(\xi)d\xi. \tag{30}$$

Note that all quantities on the right side of Eq. (30) are known from the available time series of recorded data. The Gumbel copula parameter m has been calibrated to fit joint empirical distribution $\widehat{F}_{XY}$. For the latter optimization task, the Trust-region-reflective non-linear least-squares optimization algorithm can be used, as well as the interior-point algorithm to find the minimum of the constrained non-linear multivariable function; for details, see Naess et al. [9,10]; Gaidai et al. [13] and Gao et al. [14].

Fig. 5 presents the bivariate correction scheme based on the bivariate correction method and Gumbel bivariate copula.

4. Bivariate correction results

This paper examined three mean current velocities at 0.5 and 1.0 m/s, totalling 20 sets of 4 h of simulations executed for each mean current velocity. Thus, the total simulations add up to 40 sets of 4-h simulations performed. Only two measurement channels, numbers 2 and 3, were considered from the responses of five measurement points, as shown in Fig. 1. All five measurement channels were spaced evenly and located at the bottom extending lengthwise across the SST.

Simulated R_2 and R_3 SST vessel responses were chosen as a bivariate couple since they possess a high correlation coefficient $R_{corr}=0.85$. This R_2 and R_3 SST vessel responses couple has been chosen as it was found in non-trivial, non-linear relationships, especially for large vessel rotations.

Fig. 6 presents the synchronous measurements of R_2 and R_3 SST

vessel responses. It is seen from Fig. 6 that there is a non-linear dependency between R_2 and R_3 SST vessel responses, therefore task of bivariate prediction is non-trivial.

Fig. 7 plots the bivariate results obtained for the 80 h of joint data at the two response measurement locations number 2 and 3; see Fig. 1 for measurement channel positioning. It is seen that the Gumbel logistic copula fits the bivariate empirical ACER function quite well, especially at higher probability levels with more data available, as expected.

Fig. 8 shows the ACER (averaged conditional exceedance rate) functions introduced in Eq. (22) for the longer observation period T, which is 80 h of numerical simulation, and for the shorter period $\widetilde{T} = T/10$. It is seen that, due to the high correlation between the two vessel response processes, both overestimate the ACER function levels compared with the longer dataset Naess-Gaidai curve.

The following results were obtained for the simulated SST response motions bivariate correction.

Table 2 presents the correction results for the corrected SST vessel response R_3. It is seen that the proposed correction technique resulted in remarkable improvement in accuracy, from about 20% over-prediction down to 2–3%. The return period for the predicted response level was chosen to be 40 days. The latter provides a practical example, supporting the novel correction technique introduced in this paper.

5. Conclusions

The SST is a pioneering subsea cargo drone with much research and development still to be completed. An important research area to be studied further is the collapse design of the SST's pressure hull, which is massively influenced by hydrostatic loading, a dominating load factor. This paper suggests using a bivariate correction method to examine the extreme surge and heave (positional responses) when the SST is unloading its cargo if there is a failure in the aft thrusters. The extreme motions determine the design loads experience by the SST. The extreme hydrostatic load depends on the maximum depths experienced by the extreme heave motions. Further, the minimum flowline depends on the extreme surge motions; to prevent flowline taut or snap loads. The presented study shows a practical advantage in applying the bivariate correction introduced in this paper. It brings prediction based on short time series of data quite close to the prediction based on a much longer time series. Consequently, a significant improvement in extreme value prediction accuracy is obtained. The high correlation between the two processes is a key requirement for the described correction to improve prediction accuracy. Some practical situations that may justify the analysis mentioned above would be:

- Malfunctioning of one measuring sensor while another is well-functioning.
- Another similar vessel is being designed for the same environmental condition, making the data collected from one vessel may be relevant to the other.

This paper shows that applying the bivariate correction for the cases studied has increased extreme SST vessel response prediction accuracy. This improvement shows that the proposed correction method can be useful in engineering design since having a more accurate characteristic design value is critical. Bivariate contours enable the use of bivariate design points. This distinction is different from the current practices used in the industry, which usually use a pair of uncoupled univariate design points in the same return period. This univariate design approach often results in a non-conservative design factor. While instead, the multivariate analysis extends the bivariate approach and could give a safer vessel design. The projected approach in this paper is advantageous for future emergent design for the SST, supporting dynamic parameters optimization and curtailing possible vessel damage. Moreover, such an ingenious method can also be used in other pioneering subsea drones, such as the subsea freight-glider [30,31].

Author contribution

OG: Conceptualization, Methodology, Formal analysis, Writing – original draft, Writing – review & editing. **YX**: Conceptualization, Methodology, Formal analysis, Writing – original draft, Writing – review & editing, Supervision. **RB**: Formal analysis, Writing – original draft, Writing – review & editing.

Declaration of competing interest

The authors declare that they have no known competing financial interests or personal relationships that could have appeared to influence the work reported in this paper.

References

[1] Y. Ma, Y. Xing, M.C. Ong, T. Hemmingsen, Baseline design of a subsea shuttle tanker system for liquid carbon dioxide transportation, J. Ocean Eng. 240 (2021), 109891.
[2] Equinor Energy AS. 2019. RD662093 Subsea shuttle system..
[3] Ellingsen, K.E.; Ravndal O.; Reinas, R.; Hansen, J.H.; Marra, F.; Myhre, E.; Dupuy, P.M.; Sveberg, K. 2020. RD677082 Subsea shuttle system..
[4] Norwegian Petroleum Directorate (NPD), Carbon capture and storage, Available online: http://www.norskpetroleum.no/en/environment-and-technology/carbon-capture-and-storage/, 2021. (Accessed 1 August 2021).
[5] Y. Xing, T.A.D. Santoso, Y. Ma, Technical – economic feasibility analysis of subsea shuttle tanker, J. Mar. Sci. Eng. 10 (1) (2021) 20.
[6] DNV-GL, Rules for Classification, Naval Vessels, Part 4 Sub-surface Ships, 2018 (Chapter 1) Submarines.
[7] Y. Xing, O. Gaidai, Y. Ma, A. Naess, F. Wang, A novel design approach for estimation of extreme responses of a subsea shuttle tanker hovering in ocean current considering aft thruster failure, Appl. Ocean Res. (2021) under review in.
[8] Y. Ma, M.S.D. Silva, Y.H. Xing, D. Sui, Modelling of a Subsea Shuttle Tanker Hovering in Ocean Current, Accepted in International Conference on Ocean, Offshore and Artic Engineering, 2022.
[9] A. Naess, O. Gaidai, Monte Carlo methods for estimating the extreme response of dynamical systems, J. Eng. Mech. 134 (8) (2008) 628–636.
[10] A. Naess, C. Stansberg, O. Gaidai, R. Baarholm, Statistics of extreme events in airgap measurements, J. Offshore Mech. Arctic Eng. 131 (4) (2009), 041107.
[11] A. Naess, O. Gaidai, A. Batsevych, Prediction of extreme response statistics of narrow-band random vibrations, J. Eng. Mech. 136 (3) (2010) 290–298.
[12] A. Naess, T. Moan, Stochastic Dynamics of Marine Structures, Cambridge University Press, 2013.
[13] O. Gaidai, X. Xu, A. Naess, Y. Cheng, R. Ye, J. Wang, Bivariate statistics of wind farm support vessel motions while docking, Ships Offshore Struct. 16 (2) (2020) 135–143.
[14] H. Gao, O. Gaidai, A. Naess, G. Storhaug, X. Xu, Improving container ship panel stress prediction, based on another highly correlated panel stress measurement, Mar. Struct. 64 (2018) 138–145.
[15] X. Xu, O. Gaidai, A. Naess, P. Sahoo, Improving the prediction of extreme FPSO hawser tension, using another highly correlated hawser tension with a longer time record, Appl. Ocean Res. 88 (2019) 89–98.
[16] O. Gaidai, A. Naess, X. Xu, Y. Cheng, Improving extreme wind speed prediction based on a short data sample, using a highly correlated long data, J. Wind Eng. Ind. Aerod. 188 (2019) 102–109.
[17] O. Gaidai, A. Naess, O. Karpa, X. Xu, Y. Cheng, R. Ye, Improving extreme wind speed prediction for North Sea offshore oil and gas fields, Appl. Ocean Res. 88 (2019) 63–70.
[18] A. Naess, O. Karpa, Statistics of extreme wind speeds and wave heights by the bivariate Naess-Gaidai2D method, J. Offshore Mech. Arctic Eng. 137 (2) (2015), 21602.
[19] O. Gaidai, X. Xu, J. Wang, Y. Cheng, R. Ye, O. Karpa, SEM-REV offshore energy site wind-wave bivariate statistics, Renew. Energy 156 (2020) 689–695.
[20] S. Yu, W. Wu, B. Xie, S. Wang, A. Naess, Extreme value prediction of current profiles in the South China Sea based on EOFs and the bivariate correction method, Appl. Ocean Res. 105 (2020), 102408.
[21] Q.J. Wang, A Bayesian joint probability approach for flood record augmentation, Water Resour. Res. 37 (6) (2001) 1707–1712.
[22] Y. Ma, D. Sui, Y. Xing, M.C. Ong, T.H. Hemmingsen, Depth Control Modelling and Analysis of a Subsea Shuttle Tanker. International Conference on Offshore Mechanics and Arctic Engineering, OMAE2021-61924, Virtual, 2021. Online, 21 – 30 June 2021b.
[23] D.G. Luenberger, An introduction to observers, IEEE Trans. Automat. Control 16 (6) (1971) 596–602.
[24] O. Gaidai, A. Naess, X. Xu, Y. Cheng, Improving extreme wind speed prediction based on a short data sample, using a highly correlated long data sample, J. Wind Eng. Ind. Aerod. 188 (2019) 102–109.
[25] O. Gaidai, Y. Xing, F. Wang, S. Wang, P. Yan, A. Naess, Improving extreme anchor tension prediction of a 10-MW floating semi-submersible type wind turbine, using

highly correlated surge motion record, Front. Mech. Eng. 51 (2022), https://doi.org/10.3389/fmech.2022.888497.
[26] O. Gaidai, F. Wang, Y. Wu, Y. Xing, A. Medina, J. Wang, Offshore renewable energy site correlated wind-wave statistics, Probabilist. Eng. Mech. 68 (2022), https://doi.org/10.1016/j.probengmech.2022.103207.
[27] J. Sun, O. Gaidai, F. Wang, A. Naess, Y. Wu, Y. Xing, E. van Loon, A. Medina, J. Wang, Extreme riser experimental loads caused by sea currents in the Gulf of Eilat, Probabilist. Eng. Mech. 68 (2022), https://doi.org/10.1016/j.probengmech.2022.103243.
[28] Y. Xing, O. Gaidai, Y. Ma, A. Naess, F. Wang, A novel design approach for estimation of extreme responses of a subsea shuttle tanker hovering in ocean current considering aft thruster failure, Appl. Ocean Res. 123 (2022), https://doi.org/10.1016/j.apor.2022.103179.
[29] X. Xu, F. Wang, O. Gaidai, A. Naess, Y. Xing, J. Wang, Bivariate statistics of floating offshore wind turbine dynamic response under operational conditions, Ocean Eng. 257 (2022), https://doi.org/10.1016/j.oceaneng.2022.111657.
[30] U.N. Ahmad, Y. Xing, A 2D model for the study of equilibrium glide paths of UiS Subsea Freight-Glider, IOP Conference Series, Mater. Sci. Eng. 1201 (1) (2021), 012022.
[31] Y. Xing, A conceptual large autonomous subsea freight-glider for liquid CO2 transportation, in: International Conference on Offshore Mechanics and Arctic Engineering, OMAE2021-61924, Virtual, Online, 21 – 30 June 2021, 2021.

Further Reading

[32] M.M. Barnitsas, D. Ray, P. Kinley, KT, KQ and Efficiency Curves for the Wageningen B-Series Propellers, University of Michigan, 1981.
[33] R.D. Blevins, Formulas for Natural Frequency and Mode Shape, Van Nostrand Reinhold Co., New York, 1979.
[34] A.H. Bowers, O.J. Murillo, R.R. Jensen, B. Eslinger, C. Gelzer, On Wings of the Minimum Induced Drag: Spanload Implications for Aircraft and Birds, NASA, 2016. Technical report NASA/TP-2016-219072.
[35] M. Drela, XFOIL: an analysis and design system for low Reynolds number airfoils, in: Low Reynolds Number Aerodynamics, Springer, 1989, pp. 1–12.
[36] G. Ersdal, An Overview of Ocean Currents with Emphasis on Currents on the Norwegian Continental Shelf, Norwegian Petroleum Directorate, 2001. Technical report.
[37] T.I. Fossen, Handbook of Marine Craft Hydrodynamics and Motion Control, Wiley, Chichester, West Sussex, 2011.
[38] S.F. Hoerner, Fluid-dynamic Drag: Practical Information on Aerodynamic Drag and Hydrodynamic Resistance, California, USA, 1965. Published by the author.
[39] P.L. Jamissen, Y. Ma, Y.H. Xing, Probabilistic design of ring-stiffened cylindrical hull structures applied on large cargo submarines, in: Accepted in International Conference on Ocean, Offshore and Artic Engineering, 2022.
[40] J.N. Newman, Marine Hydrodynamics, MIT Press, Massachusetts, 2017.
[41] T.T.J. Prestero, Verification of a Six-Degree of Freedom Simulation Model for the REMUS Autonomous Underwater Vehicle (Master's Thesis), Massachusetts Institute of Technology, 2001.
[42] A.J. Sørensen, Marine Cybernetics (Lecture Notes), Norwegian University of Science and Technology, Trondheim, 2018.
[43] Y. Xing, M.C. Ong, T. Hemmingsen, K.E. Ellingsen, L. Reinas, Design considerations of a subsea shuttle tanker system for liquid carbon dioxide transportation, J. Offshore Mech. Arctic Eng. 143 (4) (2021), 045001.